IET Research Journals

*Research Article*

IET Journals
The Institution of Engineering and Technology

ISSN 1751-8644
doi: 0000000000
www.ietdl.org

# Negative-Sequence Voltage Elimination for Distributed Generators in Grid-Feeding Operation Mode

*Juan M. Rey*[1], *Miguel Castilla*[2], *Jaume Miret*[2], *Manel Velasco*[3], *Pau Martí*[3], *Eduardo Mojica-Nava*[4].

[1] *Escuela de Ingenierías Eléctrica, Electrónica y de Telecomunicaciones (E3T), Universidad Industrial de Santander (UIS), Bucaramanga 680002, Colombia.*
[2] *Department of Electronic Engineering, Technical University of Catalonia (UPC), Vilanova i la Geltrú 08800, Spain.*
[3] *Department of Automatic Control, Technical University of Catalonia (UPC), Barcelona 08028, Spain.*
[4] *Department of Electrical and Electronics Engineering, Universidad Nacional de Colombia, Bogotá 111321, Colombia.*
** E-mail: juanmrey@uis.edu.co*

**Abstract:** A major concern of the power quality in distributed systems is related to the mitigation of voltage imbalances. This function can be implemented directly in the control system of the distributed generation power converters working simultaneously with the standard operation modes. This paper presents a negative-sequence voltage elimination technique for distributed generators in grid-feeding operation mode. The proposal guarantees a complete elimination of the negative-sequence voltage, while operating without a prior in-depth knowledge of the grid configuration and its characteristics. The proposed control architecture is presented together with its pseudo-code, a controller flowchart and a discussion of the implementation aspects. A closed-loop modeling is derived based on a complex transfer function approach, which is used to determine stability margins and control design guidelines. A laboratory setup was implemented to verify the performance of the proposed strategy.

## Nomenclature

*Grid-connected DG unit scheme*:

| | |
|---|---|
| $L$ | LCL filter's inverter side inductance |
| $C$ | LCL filter's capacitor |
| $L_0$ | LCL filter's grid side inductance |
| $Z_L$ | Equivalent impedance of the distribution line |
| $Z$ | Local load |
| $i_{abc}$ | Output current of the inverter |
| $v_{abc}$ | Output voltage of the DG unit |

*Notation for the $\alpha\beta$, positive- and negative-sequence components*:

| | |
|---|---|
| $x_\alpha$ | Component $\alpha$ of the variable $x$ |
| $x_\beta$ | Component $\beta$ of the variable $x$ |
| $x_{\alpha\beta}$ | Compact notation of the components $\alpha$ and $\beta$ of $x$ |
| $x_\alpha^+$ | Positive-sequence component of $x_\alpha$ |
| $x_\beta^+$ | Positive-sequence component of $x_\beta$ |
| $x_{\alpha\beta}^+$ | Compact notation of the positive-sequence components of $x_\alpha$ and $x_\beta$ |
| $x_{\mathbf{ref},\alpha}^+$ | Positive-sequence reference of $x_\alpha$ |
| $x_{\mathbf{ref},\beta}^+$ | Positive-sequence reference of $x_\beta$ |
| $x_{\mathbf{ref},\alpha\beta}^+$ | Compact notation of the positive-sequence references of $x_\alpha$ and $x_\beta$ |

*Parameters of the proposed control strategy*:

| | |
|---|---|
| $K$ | Complex gain of the control strategy |
| $K_r$ | Real component of $K$ |
| $K_i$ | Imaginary component of $K$ |

## 1 Introduction

In the last decades, distributed generation (DG) systems have increased their penetration levels in electrical grids offering benefits to the network operators such as reduction in transmission losses, more flexibility in the operation planning, and improvements in power quality services [1, 2]. Regarding this last aspect, power electronics devices play a key role in the power quality enhancement and due to this, the study of their control techniques and functionalities has gained a lot of attention from researches and industry stakeholders [3–7].

A major concern of the power quality in distributed grids is related to voltage imbalances. An imbalance can be produced by a shift between the phases of a three-phase system or by differences between its voltage amplitudes. This last case is the most frequent and is produced mainly by imbalances in loads across the grid and load operation variability [8–10].

Voltage imbalances have a major impact on weak grids compared with other type of grids, considering the significant weight of the line impedances over the voltage profile variations. If the voltage imbalances are significant (i.e., Voltage Unbalance Factor (VUF) $\geq 2.5\%$, according to [11]), they can produce undesired consequences such as increases in power losses, abnormal operation in sensitive loads and negative impacts on the life span of induction motors, power electronic converters and electronic equipment [12–14]. In addition, it is known that voltage imbalances are directly related with high ripple currents at the input DC bus of DG units, which affect power sources production [15–17].

A possibility to reduce the voltage imbalances consists of adding active power filters and STATCOMs [18–23]. However, this alternative implies adding extra equipment which represents additional costs. This problem has motivated the development of techniques to compensate the negative-sequence voltage implemented directly in the control systems of DG power converters. Thus, the DG unit can execute this auxiliary function without requiring any additional element and working simultaneously with the usual features of the grid-connected operation modes.

For the grid-feeding mode, most of the negative-sequence elimination strategies are devised for the operation during voltage sags [24–34]. In this condition, the negative-sequence control is considered together with a set of multiple functions that must be executed to guarantee ride-through capacity, which involves a trade-off in the simultaneous fulfillment of the control objectives. For this reason, these control strategies are designed to mitigate the negative-sequence until certain limit, but do not consider their total elimination. In fact, as it will be discussed later, due to the manner the current references are generated, some of them exhibit an inappropriate operation when the negative-sequence is reduced to values close to zero.

This paper proposes a technique for the negative-sequence voltage elimination in grid-feeding operation mode. Compared with previous control strategies, the proposal presents the following superior operational features:

- Due to its control architecture, the proposal allows to set directly the desired value of reduction of the negative-sequence voltage. Thus, it can be selected to guarantee the complete elimination of the imbalance or to operate under specific limits.
- The control parameters of the strategy can be designed without a prior in-depth knowledge of the grid characteristic. Due to this feature, the proper operation performance of the control strategy is ensured even if the grid presents load changes.
- Unlike other control strategies, the proposal guarantees an excellent steady-state performance even in very low values of the negative-sequence voltage. The reason for this is the used control architecture, which avoids the use of expressions that exhibits undesired behaviours when the amplitude of the negative-sequence voltage is reduced to zero.

In the paper, the control architecture is presented together with a pseudo-code and a flowchart of the control implementation. Control design guidelines are given using a modeling analysis in which an analytic expression of the complex transfer function is derived. Experimental results from a laboratory setup have been reported to validate the features and performance of the proposed control.

The rest of the paper is organized as follows, Section 2 describes the system, revisiting the basic concepts about grid-feeding operation mode. Section 3 presents the proposed control including the control architecture and its implementation. Section 4 discusses modeling while Section 5 presents design considerations. Section 6 shows the experimental results. Finally, Section 7 concludes the paper.

## 2 Distributed Generation Systems

In Fig. 1 a diagram of a grid-connected three-phase DG unit is presented. The DG unit is composed by a power source and a power inverter. In between, a DC-link is needed to balance the power flow. The inverter is connected to the grid with a LCL filter to reject harmonics and switching noise. $i_{abc}$ and $v_{abc}$ are sensed and used as input variables for the inverter controller.

The DG unit can operate in two main modes: grid-forming and grid-feeding, being the latter the focus of this paper. In grid-forming operation mode the inverter is controlled to regulate its output voltage, while in grid-feeding operation mode the inverter is controlled to inject the maximum power available or a determined power reference. The nature of the operation mode allows to model the inverter as a power-controlled current source. The basic stages of the grid-feeding operation mode controller are presented in the next subsection.

### 2.1 Grid-Feeding Operation Mode

A general control scheme for the grid-feeding operation mode is presented in Fig. 2. Voltages $v_{abc}$ and currents $i_{abc}$ are used as input variables in the control scheme. To translate $abc$ variables into $\alpha\beta 0$ domain, Clarke's transformation is applied [35]. For this end, the following conversion matrix can be used

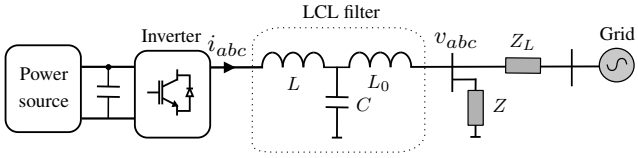


**Fig. 1.** Diagram of a grid-connected DG unit.

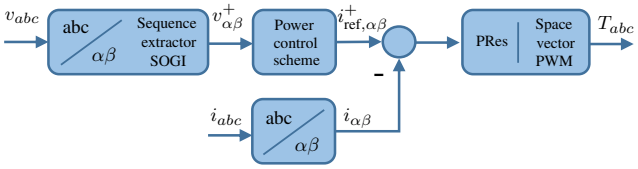


**Fig. 2.** Control scheme for grid-feeding operation mode.

$$\begin{bmatrix} x_\alpha \\ x_\beta \end{bmatrix} = \frac{1}{3}\begin{bmatrix} 2 & -1 & -1 \\ 0 & \sqrt{3} & -\sqrt{3} \end{bmatrix}\begin{bmatrix} x_a \\ x_b \\ x_c \end{bmatrix} \tag{1}$$

where $x$ must be replaced for voltages or currents, as is the case. Notice that 0 component has been omitted because a three-phase three-wire system has been considered.

It is of interest to extract both positive and negative sequences of the voltage $v_{\alpha\beta}$. For this, a Second-Order Generalized Integrator (SOGI) can be implemented to estimate these sequences [36, 37], using the following matrices:

$$\begin{bmatrix} v^+_\alpha \\ v^+_\beta \end{bmatrix} = \frac{1}{2}\begin{bmatrix} 1 & -e^{-j\frac{\pi}{2}} \\ e^{-j\frac{\pi}{2}} & 1 \end{bmatrix}\begin{bmatrix} v_\alpha \\ v_\beta \end{bmatrix} \tag{2}$$

$$\begin{bmatrix} v^-_\alpha \\ v^-_\beta \end{bmatrix} = \frac{1}{2}\begin{bmatrix} 1 & e^{-j\frac{\pi}{2}} \\ -e^{-j\frac{\pi}{2}} & 1 \end{bmatrix}\begin{bmatrix} v_\alpha \\ v_\beta \end{bmatrix}. \tag{3}$$

Conventionally, the positive-sequence current references $i^+_{\text{ref},\alpha}$ and $i^+_{\text{ref},\beta}$ are obtained using a power control scheme [38, 39], as follows

$$i^+_{\text{ref},\alpha} = \frac{2}{3}\frac{v^+_\alpha}{(v^+_\alpha)^2 + (v^+_\beta)^2}P^+_{\text{ref}} \tag{4}$$

$$i^+_{\text{ref},\beta} = \frac{2}{3}\frac{v^+_\beta}{(v^+_\alpha)^2 + (v^+_\beta)^2}P^+_{\text{ref}} \tag{5}$$

where $P^+_{\text{ref}}$ is the positive-sequence active power reference.

In the conventional approach, the reference values for the currents are obtained exclusively based on the positive-sequence. Thus, $i_{\text{ref},\alpha} = i^+_{\text{ref},\alpha}$ and $i_{\text{ref},\beta} = i^+_{\text{ref},\beta}$. These references are compared with the currents sensed values $i_\alpha$ and $i_\beta$, to calculate the errors that are the input of a proportional+resonant (PRes) controller and a space vector pulse width modulator (PWM) to obtain the control signals that drive the switches of the converter.

This standard control scheme does not include any negative-sequence voltage elimination. Thus, if any type of imbalance is produced on the grid, a negative-sequence component will be presented at the DG output voltage. In the following subsection, the conventional approaches to address this issue are presented.

### 2.2 Conventional Negative-Sequence Elimination Approach

In general, most of the conventional negative-sequence reduction strategies are based on the introduction of negative-sequence current references $i^-_{\text{ref},\alpha}$ and $i^-_{\text{ref},\beta}$, which are added to the positive-sequence references, as

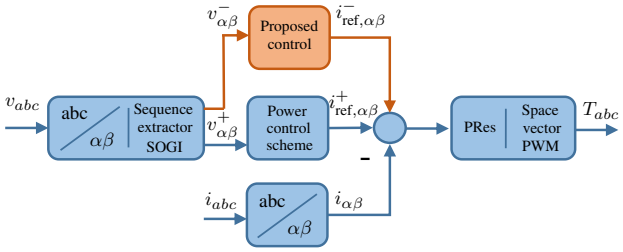


**Fig. 3.** Control scheme for grid-feeding operation mode including the proposed control block.

$$i_{\text{ref},\alpha} = i^+_{\text{ref},\alpha} + i^-_{\text{ref},\alpha} \tag{6}$$

$$i_{\text{ref},\beta} = i^+_{\text{ref},\beta} + i^-_{\text{ref},\beta}. \tag{7}$$

These references are calculated using similar power control schemes to (4) and (5), but considering negative-sequence variables. The schemes presented in [31–34] can be expressed in a general form as

$$i^-_{\text{ref},\alpha} = \frac{2}{3}\frac{v^-_\alpha}{(v^-_\alpha)^2+(v^-_\beta)^2}P^-_{\text{ref}} + \frac{2}{3}\frac{v^-_\beta}{(v^-_\alpha)^2+(v^-_\beta)^2}Q^-_{\text{ref}} \tag{8}$$

$$i^-_{\text{ref},\beta} = \frac{2}{3}\frac{v^-_\beta}{(v^-_\alpha)^2+(v^-_\beta)^2}P^-_{\text{ref}} - \frac{2}{3}\frac{v^-_\alpha}{(v^-_\alpha)^2+(v^-_\beta)^2}Q^-_{\text{ref}} \tag{9}$$

where $P^-_{\text{ref}}$ and $Q^-_{\text{ref}}$ are negative-sequence active and reactive power references, correspondingly.

As an alternative approach, (8) and (9) are formulated using the amplitude of the negative-sequence currents associated with the active and reactive powers, as

$$i^-_{\text{ref},\alpha} = \frac{v^-_\alpha I^-_P}{V^-} + \frac{v^-_\beta I^-_Q}{V^-} \tag{10}$$

$$i^-_{\text{ref},\beta} = \frac{v^-_\beta I^-_P}{V^-} - \frac{v^-_\alpha I^-_Q}{V^-} \tag{11}$$

being $I^-_P = \frac{2}{3}\,(P^-_{\text{ref}} \,/\, V^-)$ and $I^-_Q = \frac{2}{3}\,(Q^-_{\text{ref}} \,/\, V^-)$.

Notice that in both strategies (8), (9) and (10), (11), the current references are calculated based on expressions that include the negative-sequence voltage amplitude in the denominator. For this reason, when this value is reduced to almost zero, the DG operates exhibiting an undesired variable behaviour. This feature limits the negative-sequence reduction, making its total elimination unfeasible. In the following Section a control technique that overcomes this drawback is proposed.

## 3 Proposed Control Technique

This Section presents the proposed control and a discussion on its implementation aspects.

### *3.1 Control Architecture*

The aim of the control strategy is to generate a negative-sequence current reference $i^-_{\text{ref},\alpha\beta}$ to effectively eliminate the negative-sequence output voltage $v^-_{\alpha\beta}$, which is used as input variable. As a benchmark, a voltage reference is defined as $v^-_{\text{ref},\alpha\beta}$. It is of interest to eliminate the error $\varepsilon^-_{\alpha\beta}$ defined as

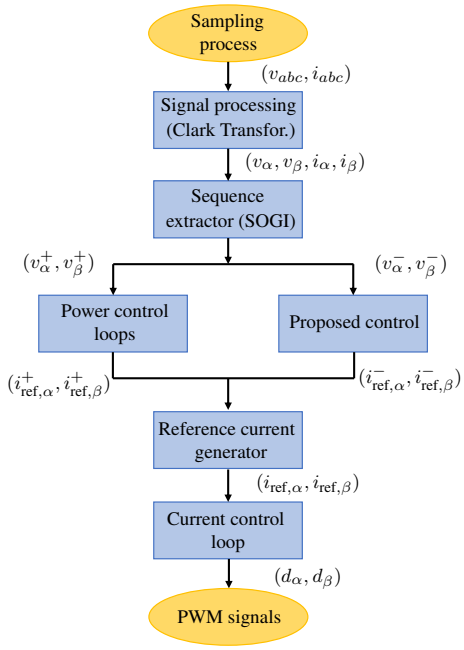


**Fig. 4.** Flowchart of the controller including the proposed control strategy.

$$\varepsilon^-_{\alpha\beta} = v^-_{\text{ref},\alpha\beta} - v^-_{\alpha\beta}. \tag{12}$$

Notice that, as the objective is to suppress the negative sequence, i.e., lead $v^-_{\alpha\beta}$ to zero, it is expected to set $v^-_{\text{ref},\alpha\beta} = 0$. However, the proposal is presented in a general form for the case that this reference is established at a non-zero value (below an established operational limit).

The control strategy is based on the integration of $\varepsilon^-_{\alpha\beta}$. Due to the rotative nature of this phasorial variable, it is proposed the use of an operator which allows to set a rotative framework for the integration. As $\varepsilon^-_{\alpha\beta}$ rotates at frequency $-\omega$, an operator $e^{j\omega t}$ that multiplies this variable will have a cancellation effect on the rotation. Once the result of the integral control action is calculated, the signal is rotated again (using the operator $e^{-j\omega t}$) to be implemented into the system as a negative-sequence reference. The proposed strategy can be mathematically described as follows

$$i^-_{\text{ref},\alpha\beta} = K\, e^{-j\omega t} \int e^{j\omega t}\,(v_{\text{ref},\alpha\beta} - v^-_{\alpha\beta})\, dt \tag{13}$$

where $K \in \mathbb{C}$ is a control parameter.

Fig. 3 presents the general control scheme including the block of the control proposal. This strategy is complementary to the standard control scheme, and does not modify any other control block, being easily adaptable to different operational environments. Further details about the implementation aspects are discussed in the following subsection.

### *3.2 Implementation Features*

The suitable implementation of the proposed control requires the discretization of the equations that compose the strategy. Also, considering the complex nature of the variables and parameters, it is recommended to follow an implementation approach based on channels, in order to conveniently separate the $\alpha\beta$ variables.

As stated in (13), the parameter $K$ is a complex number, and it can be defined as $K = K_r + jK_i$. This alternative provides two degrees of freedom to the control design and, as it will be discussed later, it allows obtaining dynamic properties that can not be easily achieved with a real parameter.

**TASK** : controller($h$)

/* Definition of complex numbers product function */

$(y_r, y_i)$ = CNP$(x_r, x_i, z_r, z_i)$

$y_r = x_r z_r - x_i z_i$ ; $y_i = x_r z_i + x_i z_r$

/* Sampling and processing */

$(v_{abc}, i_{abc})$ = ReadADC()

$(v_\alpha, v_\beta)$ = Clarke$(v_{abc})$

$(i_\alpha, i_\beta)$ = Clarke$(i_{abc})$

/* Sequence extractor SOGI */

$(v_\alpha^+, v_\beta^+, v_\alpha^-, v_\beta^-) = \text{SOGI}(v_\alpha, v_\beta)$

/* Power control loop */

$i^+_{\text{ref},\alpha} = \frac{2}{3}\frac{v_\alpha^+}{(v_\alpha^+)^2+(v_\beta^+)^2} P^+_{\text{ref}}$ ; $i^+_{\text{ref},\beta} = \frac{2}{3}\frac{v_\beta^+}{(v_\alpha^+)^2+(v_\beta^+)^2} P^+_{\text{ref}}$

/* Proposed control */

$\varepsilon_\alpha^- = v^-_{\text{ref},\alpha} - v_\alpha^-$ ; $\varepsilon_\beta^- = v^-_{\text{ref},\beta} - v_\beta^-$

$(C1_\alpha, C1_\beta)$ = CNP$(\cos(\omega T_0), \sin(\omega T_0), \varepsilon_\alpha^-, \varepsilon_\beta^-)$

$\lambda_\alpha = \lambda_\alpha + T_0 C1_\alpha$ ; $\lambda_\beta = \lambda_\beta + T_0 C1_\beta$ % Discretized integral

$(C2_\alpha, C2_\beta)$ = CNP $(\cos(-\omega T_0), \sin(-\omega T_0), \lambda_\alpha, \lambda_\beta)$

$(i^-_{\text{ref},\alpha}, i^-_{\text{ref},\beta})$ = CNP$(K_r, K_i, C2_\alpha, C2_\beta)$

/* Reference current generator */

$i_{\text{ref},\alpha} = i^+_{\text{ref},\alpha} + i^-_{\text{ref},\alpha}$ ; $i_{\text{ref},\beta} = i^+_{\text{ref},\beta} + i^-_{\text{ref},\beta}$

/* Current control loop */

$d_\alpha = \text{PRes}(i_{\text{ref},\alpha} - i_\alpha)$ ; $d_\beta = \text{PRes}(i_{\text{ref},\beta} - i_\beta)$

$(T_{abc})$ = SpaceVectorPWM$(d_\alpha, d_\beta)$

**Fig. 5.** Pseudo-code of the controller including the proposed control strategy.

The exponential terms in (13) are disaggregated using Euler's formula (i.e., $e^{jx} = \cos(x) + j\sin(x)$). Also, to facilitate the implementation, a function that calculates the product of complex numbers is recommended (i.e., assuming two complex numbers $x_r + jx_i$ and $z_r + jz_i$, the product is defined as $y_r + jy_i$ being

$$y_r = x_r z_r - x_i z_i \tag{14}$$

$$y_i = x_r z_i + x_i z_r \tag{15}$$

Fig. 4 shows a flowchart that allows a better understanding of the way in which the sampling signals are processed in order to calculate the key variables of the control strategy. Furthermore, in Fig. 5, a step-by-step pseudo-code of the proposed control scheme is shown, considering a discrete step of $T_0$. In the next subsection, the modeling and design considerations are addressed.

## 4 Closed-loop Dynamic Model

In this Section, a closed-loop dynamic model for the DG unit is derived. This model is used for the design of the proposed control.

### 4.1 Modeling of the System

The focus of this section is on the modeling of the negative-sequence components. To this end, the positive-sequence components are considered as perturbing signals to the negative-sequence channel. This separation in channels allows to find the closed-loop poles of the negative-sequence voltage dynamics and, therefore, to properly design the control parameter $K$.

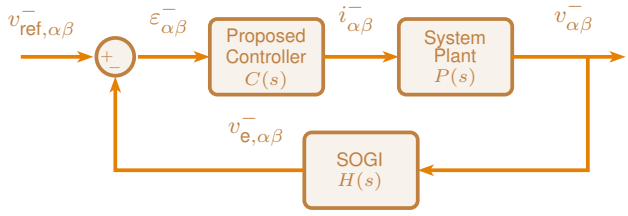


**Fig. 6.** Closed-loop model for the negative-sequence channel.

Fig. 6 shows the closed-loop model for the negative-sequence channel. As input variable, the model considers the voltage reference $v^-_{\text{ref},\alpha\beta}$, while the output variable is the voltage $v^-_{\alpha\beta}$. These are complex variables representing the components $\alpha$ and $\beta$ in a compact notation. The definition of each modeling block is presented below. A perfect tracking between the reference current and the injected current is considered (i.e, $i^-_{\text{ref},\alpha\beta} = i^-_{\alpha\beta}$) [40]. This is defined assuming a correct design of the control parameters, guaranteeing a decoupling of the dynamics of the different control loops.

*4.1.1 Proposed Controller Block:* The proposed control has as input variable the error $\varepsilon^-_{\alpha\beta}$ and as output variable the current reference $i^-_{\text{ref},\alpha\beta}$ ($i^-_{\alpha\beta}$ according to the perfect tracking assumption). For modeling purposes, consider the first-time derivative of (13), which is equal to

$$\dot{i}^-_{\text{ref},\alpha\beta} = -j\omega\, i^-_{\text{ref},\alpha\beta} + K\, \varepsilon^-_{\alpha\beta}. \tag{16}$$

Converting this expression to the frequency domain, it is possible to obtain the following transfer function

$$C(s) = \frac{i^-_{\alpha\beta}}{\varepsilon^-_{\alpha\beta}} = \frac{K}{s + j\omega}. \tag{17}$$

*4.1.2 SOGI Sequence Extractor Block:* The modeling of the SOGI is obtained based on the works presented in [40–42]. The inclusion of this block allows to consider the effect of the sequence extraction into the system dynamics. The voltage signal $v^-_{\alpha\beta}$ is used as input variable, while the estimated negative-sequence voltage $v^-_{\text{e},\alpha\beta}$ is the output variable.

Using the averaged model presented in [42], it is possible to obtain the following equations

$$\begin{bmatrix} v^-_{\text{e},\alpha} \\ v^-_{\text{e},\beta} \end{bmatrix} = \frac{1}{s^2 + 2\xi\omega s + \omega^2} \begin{bmatrix} \xi\omega s & \xi\omega^2 \\ -\xi\omega^2 & \xi\omega s \end{bmatrix} \begin{bmatrix} v^-_\alpha \\ v^-_\beta \end{bmatrix}. \tag{18}$$

This expression can be equivalently described by the complex transfer function [43]

$$H(s) = \frac{v^-_{\text{e},\alpha\beta}}{v^-_{\alpha\beta}} = \frac{\xi\omega s - j\xi\omega^2}{s^2 + 2\xi\omega s + \omega^2}. \tag{19}$$

The parameter $\xi$ in (19) is calculated as discussed in [42], using the design guideline $\xi = 5/(\omega t_s)$, being $t_s$ the settling time of the SOGI, considered in this work as $t_s = 16.7$ ms, i.e., one period of the power grid frequency.

*4.1.3 System Plant Block:* The scheme of the system is presented in Fig.1. The distribution line and the local load, $Z_L$ and $Z$, are considered balanced. The imbalance is generated by the grid voltage $V_{grid}$. In frequency domain, the output voltage and the output current are represented as $V$ and $I$, respectively. Assuming $Z >> Z_L$ and, therefore, $Z \parallel Z_L \approx Z_L$ (which is valid for the

**Table 1** Parameters of the experimental setup

| Element | Symbol | Quantity |
|---|---|---|
| Nominal frequency | $\omega_0$ | $120\pi$ rad/s |
| Nominal voltage | $V_0$ | 110 V rms |
| LCL inverter side inductance | $L$ | 5 mH |
| LCL capacitor | $C$ | 1.5 $\mu$F |
| LCL grid side inductance | $L_0$ | 1 mH |
| Line impedance | $Z_L$ | 0.5 + j 1.73 $\Omega$ |
| Resistance of $Z_L$ | $R_L$ | 0.5 $\Omega$ |
| Inductance of $Z_L$ | $L_L$ | 4.6 mH |
| Local load impedance | $Z$ | 24.2 $\Omega$ |
| SOGI parameter | $\xi$ | 0.7958 |
| Positive-sequence active power reference | $P^+_{\text{ref}}$ | 1000 W |

**Table 2** Stability ranges for parameters $K_i$ and $K_r$

| Value of the parameter $K_i$ | Range for the parameter $K_r$ |
|---|---|
| -2.5 | Unstable |
| 0.0 | $0.0 < K_r < 12.0$ |
| 2.5 | $-9.8 < K_r < 21.6$ |
| 5.0 | $-15.6 < K_r < 27.0$ |
| 7.5 | $-20.2 < K_r < 31.1$ |

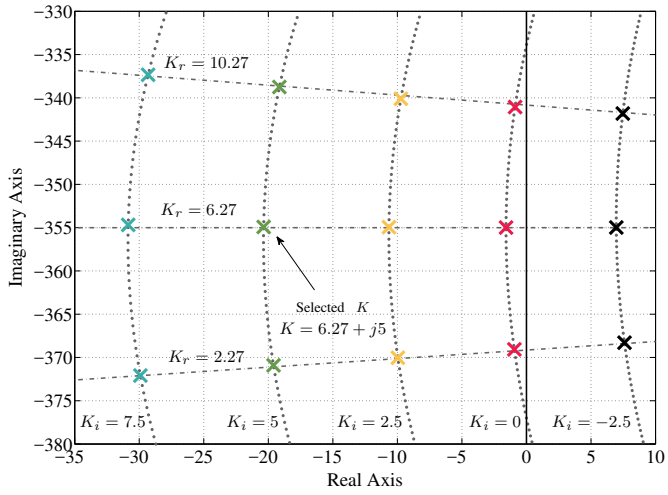


**Fig. 7.** Location of the dominant closed-loop poles for different values of $K$.

setup built for the experimental tests presented in Section 6), the output voltage can be written in frequency domain as

$$V = (R_L + L_L s)I + V_{grid} \tag{20}$$

where $R_L$ and $L_L$ are the resistance and inductance of $Z_L$, respectively. To obtain the model of the system plant, the unbalanced grid voltage $V_{grid}$ can be seen as a perturbation. To consider the dynamics of the system, a dynamic phasor approach is suggested [44, 45]. Then, obtaining the complex transfer function for the negative-sequence channel, the plant can be modeled as

$$P(s) = \frac{v^-_{\alpha\beta}}{i^-_{\alpha\beta}} = R_L + L_L s - j\omega L_L. \tag{21}$$

## 5 Control Design

In this Section, the design of the control parameters is presented. First, the closed-loop stability is analyzed. Then, design guidelines are discussed. Finally, a sensitivity analysis is presented, to determine the impact of the grid impedance variations over the position of the dominant closed-loop pole.

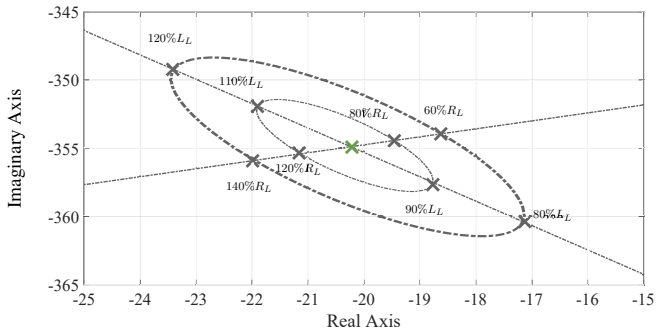


**Fig. 8.** Location of the dominant closed-loop pole with $K = 6.27 + j5$ considering variations in the line impedance values $R_L$ and $L_L$.

### 5.1 Closed-loop Stability Analysis

From Fig. 6, the closed-loop complex transfer function of the system can be written as

$$F(s) = \frac{P(s)C(s)}{1 + P(s)C(s)H(s)}. \tag{22}$$

The models derived for the system plant (21), SOGI (19) and proposed control (17) can be inserted in (22) to obtain the closed-loop dynamics of the system. The complete expression and coefficients of $F(s)$ are presented in Appendix 9.1. The numerical values of the coefficients are obtained using the parameters of the experimental setup in Table 1. Since a complex transfer function was considered, the characteristic polynomial of the closed-loop system, $q(s) = 1 + P(s)C(s)H(s)$, is a polynomial with complex coefficients. In order to determine if the closed-loop system is stable for some values of the control parameter $K$, a Generalized Routh-Hurwitz (GRH) criterion is used. This extended criterion was initially presented in [46], and recently in [47] for an induction generator. Consider a third order polynomial with complex coefficients of the general form

$$q(s) = c_0 s^3 + (c_1 + jd_1)s^2 + (c_2 + jd_2)s + (c_3 + jd_3) \tag{23}$$

where $c_0$ is assumed to be real and positive. Then, the GRH criterion for a third order polynomial with complex coefficients is presented in the following Lemma [46].

**Lemma 1.** *Considering a cubic polynomial with complex coefficients (23), the roots are in the open left-half plane if and only if the determinants $\Delta_i$ are strictly positive for $i = 1, 2, 3$, where*

$$\Delta_1 = c_1, \quad \Delta_2 = \det\begin{pmatrix} c_1 & c_3 & -d_2 \\ c_0 & c_2 & -d_1 \\ 0 & d_2 & c_1 \end{pmatrix},$$

$$\Delta_3 = \det\begin{pmatrix} c_1 & c_3 & 0 & -d_2 & 0 \\ c_0 & c_2 & 0 & -d_1 & -d_3 \\ 0 & c_1 & c_3 & 0 & -d_2 \\ 0 & d_2 & 0 & c_1 & c_3 \\ 0 & d_1 & d_3 & c_0 & c_2 \end{pmatrix}.$$

Now, using Lemma 1 to analyze the roots of the complex closed-loop polynomial $q(s)$, some analytical conditions for stability can be obtained. For a first case, considering $K_i = 0$, from $\Delta_1 = c_1$, it is guaranteed that $\Delta_1 > 0$ for any $K_r > \frac{-2}{L_L}$. For $\Delta_2 > 0$, it is obtained that any $K_r > 0$ satisfies the condition. Finally, for $\Delta_3 > 0$, according to the numerical values, it is obtained that the range $0 < K_r < 12$ guarantees closed-loop system stability.

To illustrate all possibilities of the complex parameter $K$, several simulations similar to root-locus are performed. Fig. 7 shows the results for the dominant (low-frequency) pole. The other two poles are not considered in the plot because they are located at high frequencies of the x-axis left-hand plane (stable for a large range of

values of $K$ and with a fast dynamic response). The curves for $K_i$ equal to $-2.5$, 0, 2.5, 5 and 7.5, are indicated in the Figure, while the values of the ranges for $K_r$ in which the dominant pole is stable are presented in Table 2.

As can be observed, there are many values of the control parameters that guarantee the stability conditions. However, according to the position of the dominant pole the system presents different dynamic response performance. The selection of the values of the control parameters $K_r$ and $K_i$ must be done according to desired dynamic characteristics. Design guideline are presented in the following subsection.

### 5.2 Design Guidelines

According to Fig. 7, the increase in the value of the parameter $K_i$ produces a shift to the left in the position of the dominant pole. It is desirable to obtain a fast speed of response without affecting the internal loops of the control and avoiding the risk of losing the dominance of the pole. Thus, as a design guideline for the control parameter $K_i$, it is recommended to select a position of the pole to reach a response time approximately ten times slower than the dynamics of the internal control loops.

Furthermore, another important aspect that can be concluded is that all the curves with constant values of $K_i$ have a similar concave shape, whose vertices correspond to the same value of $K_r$. As the vertex is the left most possible point of each curve (i.e., the maximum speed of response of the curve), the recommended design guideline is to select this position as the value for the control parameter $K_r$.

For the numerical example presented in the paper, the control parameter is chosen as $K = 6.27 + j5$. It is important to notice that the dominant pole can be located in a region to met the above design guidelines, therefore, there is no a single optimal location that must be selected. Fifteen points of operation are highlighted with X's in the plot, which are evaluated in the next section in order to verify if the modeling effectively corresponds to the experimental results obtained.

### 5.3 Impact of the Grid Impedance Variations

A sensitivity analysis was carried out to evaluate the impact of the variation in the value of the line impedance $Z_L$ (i.e., the resistance $R_L$ and the inductance $L_L$) over the position of the dominant closed-loop pole. Considering a chosen control parameter, $K = 6.27 + j5$, Fig. 8 presents the position of the dominant pole for different deviations of the values of $R_L$ and $L_L$ (with respect to the values used in the design procedure presented in Table 1). The value $R_L$ was deviated $\pm 20\%$ and $\pm 40\%$, while $L_L$, $\pm 10\%$ and $\pm 20\%$. The new positions of the dominant pole are marked with gray X's.

The results show no significant impacts over the position of the dominant pole even with a line impedance variation of 40%. Basically, this means that an appropriate design of the control parameters can be performed without requiring an "in-depth" knowledge of the grid impedance (understood as an accurate estimation and with low margin of error). An estimated value of the grid impedance can be obtained using any online grid calculation method presented in the literature, see, e.g., [48–52]. Many of these methods are easy to implement, do not require large computation capacity and allow to obtain accurate results in short operation times.

It is worth mentioning that these changes on the position of the dominant pole are exclusively related to the transient dynamics of the negative-sequence elimination. Due to the nature of the control strategy, in all the cases when the dominant pole is stable, a complete elimination of the negative-sequence voltage is guaranteed, as will be verified in the experimental results of the next section.

## 6 Experimental Results

The experimental tests were performed in the laboratory prototype that is shown in Fig. 9. The setup follows the scheme depicted in Fig. 1. The DG unit was implemented using a DC power

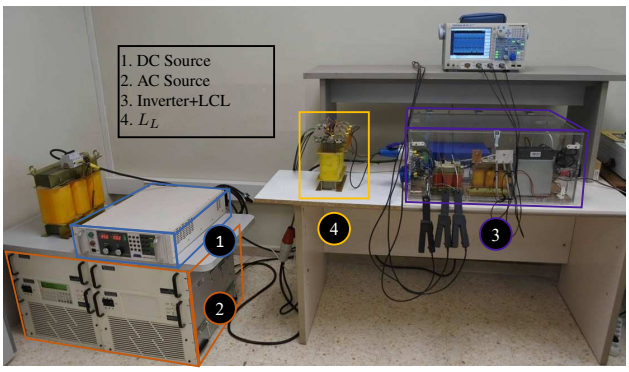


**Fig. 9.** Experimental setup.

source (AMREL SPS-800-12), which emulates the power generation, a MTLCBI0060F12IXHF GUASCH three-phase IGBT full-bridge power inverter and a LCL output filter. A Texas Instruments TMS320F28335 floating-point digital-signal processor was used as control platform. The data was gathered in a PC to be plotted using Matlab. The distribution line $Z_L$ was emulated with a RL impedance, while the local load $Z$ corresponds to a resistive load. For the tests presented in subsections 6.1 to 6.4 were considered balanced impedances for the local load $Z$ and the line $Z_L$, while specific unbalance scenarios were implemented in the tests presented in subsections 6.5 and 6.6. Finally, regarding the grid, a Pacific Power AC grid emulator was used operating in unbalanced conditions. The phase amplitudes of the grid were programmed to produce positive- and negative-sequence DG output voltages of $V^+ = 151.7\ V$ and $V^- = 4.3\ V$ (VUF = 2.83 %). The rest of the parameters related to the experimental setup were presented in Table 1.

### 6.1 Conventional Negative-Sequence Elimination Approach

First, a test using the conventional negative-sequence elimination approach was performed. To this end, the negative-sequence current references in (10) and (11) were implemented considering $I_P^- = 0$ and $I_Q^- = 5$. The experimental results are presented in Fig. 10. The test begins with the DG unit connected to the grid, with the negative-sequence control disabled. At $t = 0.2$ s, the control is activated and the negative-sequence voltage is gradually reduced. The results clearly show that the strategy exhibits an undesired performance when $V^-$ is reduced to values close to zero. The rippling behaviour presents maximum peaks that reach $V^- = 1.24\ V$. This value corresponds to almost 30% of the amplitude of the negative-sequence before the control strategy activation. Even if these values are reached instantly, it is possible to conclude that the operation of this type of control strategies is not suitable when $V^-$ is highly reduced. As previously discussed, this is due to the nature of the control strategy scheme.

### 6.2 Proposed Control Strategy Using Different Gains $K$

To verify the performance predictions of the modeling section, Fig. 11 presents $V^-$ for different tests using the values of the control parameter $K$ highlighted in Fig. 7. To clearly distinguish the position of the dominant pole associated with each test, the same colors have been used in both figures.

The results obtained are consistent with the modeling. The tests using $K_i = -2.5$ present unstable responses. On the other tests, with $K_i \geq 0$, the results show stable dynamics with different speed of responses. Notice how in each set of tests with the same $K_i$, the test with $K_r = 6.27$ has always the faster dynamic response. The reason is that, in this case, the real part of the dominant pole is greater, as it was pointed out in the discussion of Fig. 7. Furthermore, the tests make it clear that the increase in the value of the parameter $K_i$ has an impact over the speed of response.

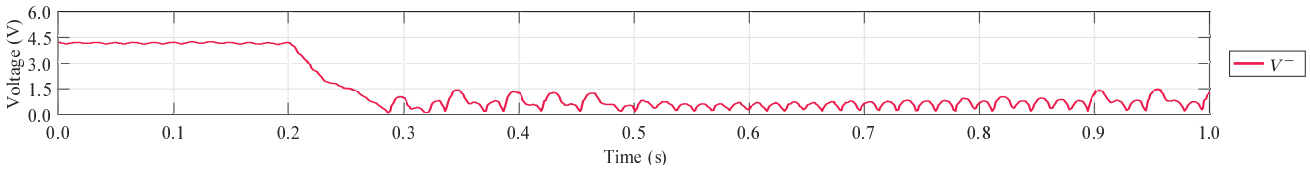


**Fig. 10.** Amplitude of the negative-sequence voltage $V^-$ using the conventional negative-sequence voltage elimination approach.

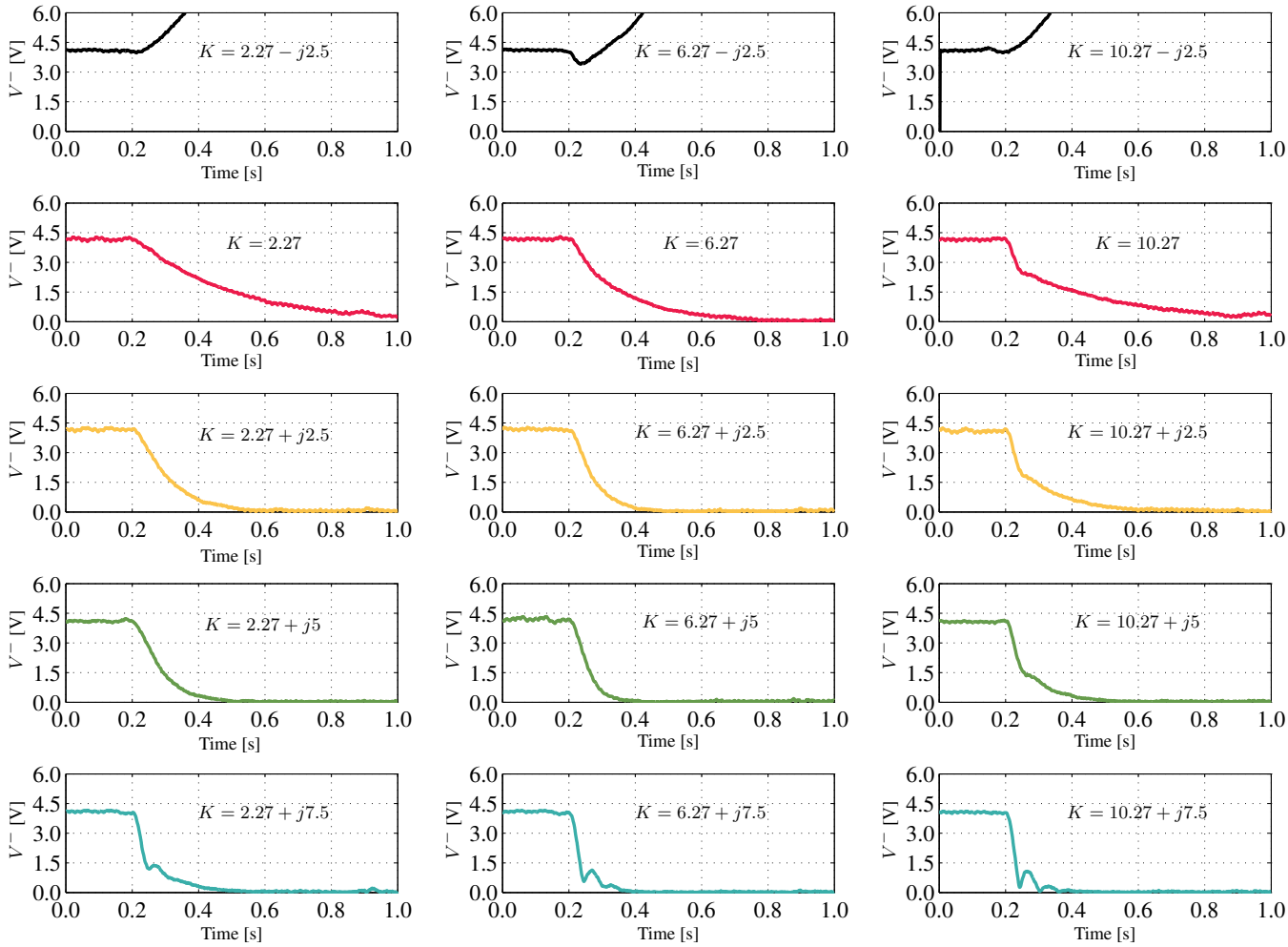


**Fig. 11.** Amplitude of the negative-sequence voltage using the proposed control strategy with different values of $K$.

The selected value of the parameter (i.e., $K = 6.27 + j5$) presents a speed of response of approximately 0.17 s. As it can be seen, for greater values of $K_i$ a faster speed of response is obtained. However, there is a coupling with the internal control loops, producing undesired oscillations in the transient response, illustrated in Fig. 11 for $K_i = 7.5$.

### *6.3 Proposed Control Strategy - Base case*

To verify the performance of the proposed control strategy, different tests cases were implemented. First, in this section is presented the base case. This scenario is characterized by two aspects: (a) The local load $Z$ and the line impedance $Z_L$ are balanced, as considered in subsection 4.1.3, (b) the positive-sequence active power reference $P^+_{\text{ref}}$ is constant during all the test. Variations of these operating characteristics were considered in other tests, as will be described in the following subsections. The control parameter was implemented using the selected value $K = 6.27 + 5j$.

In Fig. 12(a) the amplitude of the negative-sequence voltage is shown. Voltages $V_{abc}$ are not presented because is difficult to observe the imbalance in this type of signals. Instead of these voltages, the $\alpha\beta$ components of the negative-sequence voltage are depicted in Fig. 12(b). The test begins with the DG unit connected to the grid and the proposed control disabled. Before the control strategy activation, the amplitude of the negative-sequence is uncontrolled and presents its maximum value, $V^- = 4.3\ V$. At $t = 0.2$ s, the control is activated, which produces a gradually reduction of the negative-sequence voltage. Both figures clearly show that this control action is carried out smoothly and without significant overshoots. After approximately 0.17 s, the negative-sequence voltage is considered completely eliminated.

Once the steady-state is reached, the rippling behaviour presents a peak of maximum $V^- = 0.05\ V$, which corresponds to less than 1.2% of the initial value of the negative-sequence before the control strategy activation. This value is so small that it is negligible, and the negative-sequence is considered eliminated. This feature constitutes one of the main differences that distinguish the superior behavior of the proposed control strategy over other proposals in the literature.

Fig. 12(c) presents the output currents of the inverter $i_{abc}$. This figure allows to appreciate the differences in the operation of the currents before and after the control strategy activation. To observe

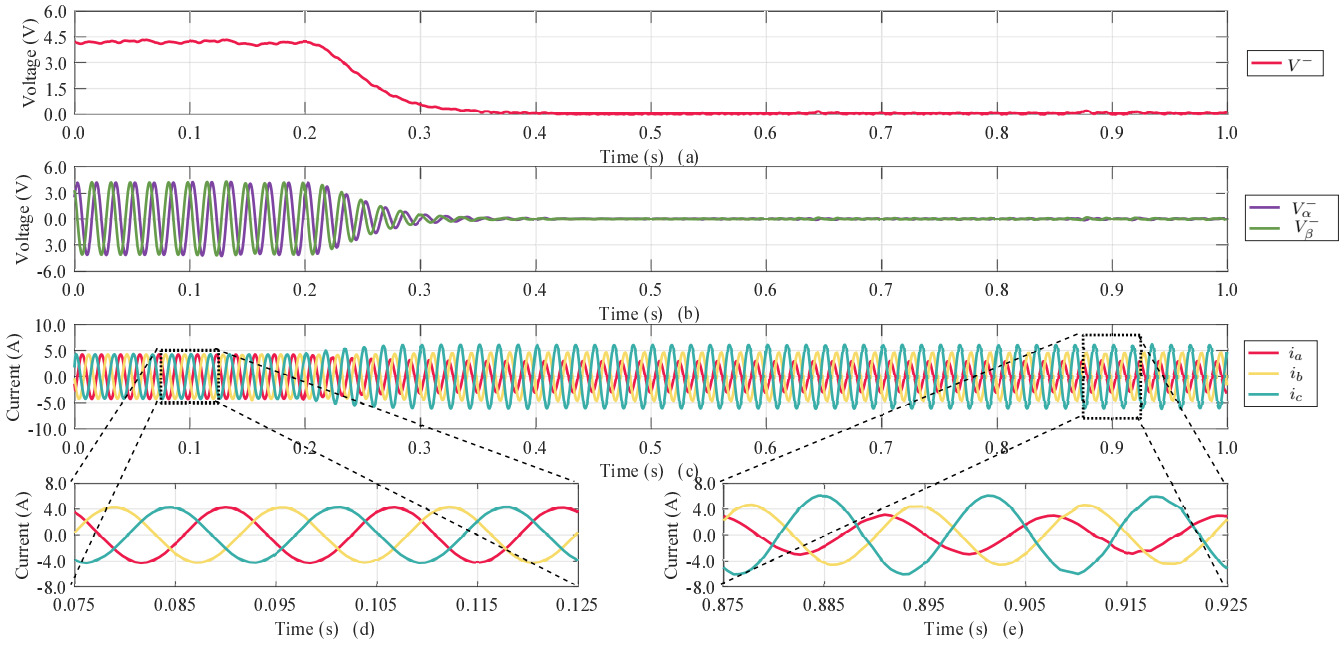


**Fig. 12.** Experimental results of the proposed control with $K = 6.27 + j5$: (a) amplitude of the negative-sequence voltage $V^-$, (b) $\alpha\beta$ components of the negative-sequence voltage $V^-_{\alpha\beta}$, (c) output phase currents $i_a$ $i_b$ $i_c$, and (d) and (e) two zoom-in of the output phase currents.

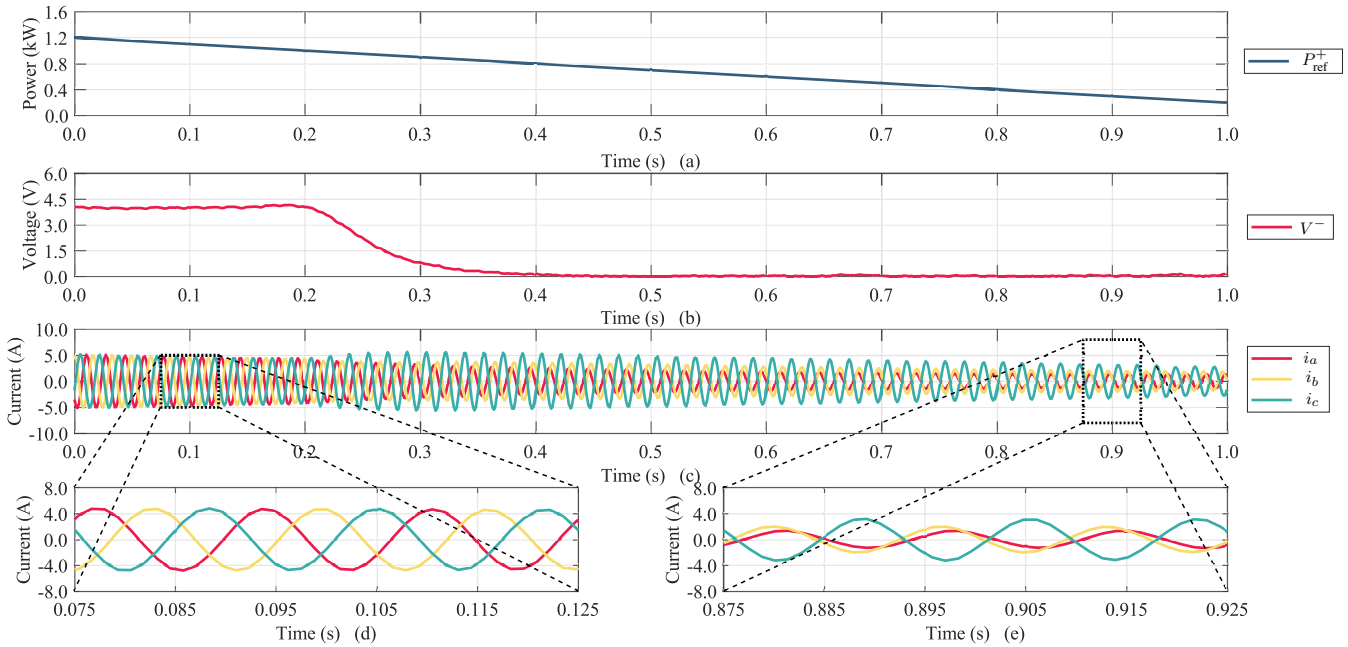


**Fig. 13.** Experimental results of the proposed control with $K = 6.27 + j5$ considering variable energy production: (a) Positive-sequence active power reference $P^+_{\text{ref}}$, (b) amplitude of the negative-sequence voltage $V^-$, (c) output phase currents $i_a$ $i_b$ $i_c$, and (d) and (e) two zoom-in of the output phase currents.

the detail of the three-phase currents in a clearer way, two selected zoom-in are shown in Fig. 12(d) and Fig. 12(e).

In the first stage of the test, while the control strategy is deactivated (the axis of the zoom in Fig. 12(d) covers the time interval 0.075 s $\leq t \leq$ 0.125 s) the currents injected to the grid are balanced and no negative-sequence correction is applied. Once the proposed control is activated and the steady-state is reached (the axis of the zoom in Fig. 12(e) covers the time interval 0.875 s $\leq t \leq$ 0.925 s), the currents injected to the grid are unbalanced, which correspond to the correction mechanism that allows the elimination of the negative-sequence output voltage.

### *6.4 Proposed Control Strategy - Variable Energy Production*

In this test, the proposed control strategy is evaluated considering variable energy production. This characteristic is emulated through the variation of the positive-sequence active power reference $P^+_{\text{ref}}$, which was programmed to decrease linearly starting with a value of 1200 W. Regarding the control parameter, it was considered a value of $K = 6.27 + j5$. The experimental results are presented in Fig. 13.

In Fig. 13(a), the value of $P^+_{\text{ref}}$ is depicted. Similarly to previous tests, the control strategy starts disabled and is activated at $t =$

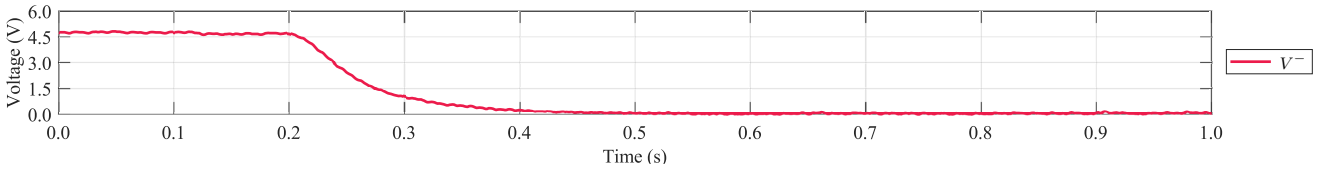


**Fig. 14.** Experimental results of the proposed control with $K = 6.27 + j5$ and considering unbalanced line impedance $Z_L$: Amplitude of the negative-sequence voltage $V^-$.

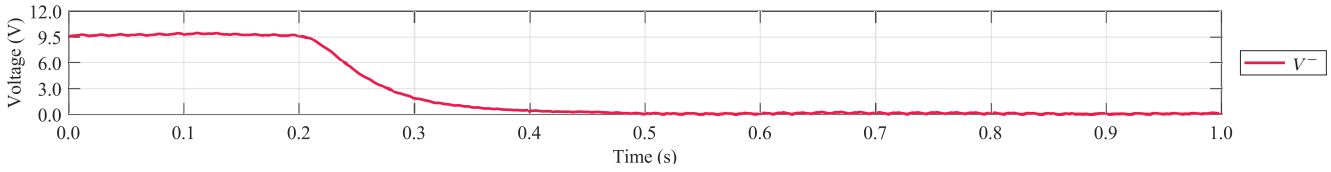


**Fig. 15.** Experimental results of the proposed control with $K = 6.27 + j5$ and considering unbalanced local load $Z$: Amplitude of the negative-sequence voltage $V^-$.

0.2 s. Thus, the variation of $P^+_{\text{ref}}$ occurs before and after the activation of the control strategy. The amplitude of the negative-sequence voltage is shown in Fig. 13(b). As can be seen, the variability in energy production does not affect the ability to eliminate the negative-sequence voltage, nor its operational characteristics (e.g., the transient dynamics).

Fig. 13(c) presents the output currents of the inverter $i_{abc}$. In this figure is possible to observe how the reduction in $P^+_{\text{ref}}$ impacts over the amplitudes of the currents producing a linear decrease. Selected zoom-in are shown in Fig. 13(d) and Fig. 13(e). The first figure shows the currents $i_{abc}$ before the control activation. Because there is no control mechanism over the negative-sequence voltage, the currents are balanced during this time interval. The second figure shows the currents $i_{abc}$ after the activation of the control mechanism. Notice how the reduction on the positive-sequence active power simultaneously with the negative-sequence voltage elimination control, impact over the phases of the currents. In this way, the currents are adapted to the control objectives of the upper loops.

### *6.5 Proposed Control Strategy - Unbalanced Line Impedance $Z_L$*

In all the tests presented above were considering balanced impedances for $Z$ and $Z_L$. Because of this, the imbalance presented was generated exclusively by the differences in the phases of the grid. In this test, an imbalance was introduced in the line impedance $Z_L$ (keeping the grid unbalanced) to evaluate the performance of the proposed control in this type of scenarios. The imbalance was introduced in phase C of $Z_L$. While the phases A and B operate at the value that had been previously used (i.e., 0.5 + j 1.73 Ω, see Table 1), phase C has been modified, reducing its inductance to operate in a value of 0.5 + j 0.98 Ω (i.e., $L_L$ = 2.6 mH).

Fig. 14 presents $V^-$ for the experimental test. The results show that the imbalance before the control strategy activation is $V^- = 4.7\ V$, a greater value compared with the previous test, due to the impact of the unbalanced line impedance. Once the control strategy is activated at $t = 0.2$ s, the negative-sequence voltage is completely eliminated with similar performance characteristics to those observed in the previous tests.

### *6.6 Proposed Control Strategy - Unbalanced Local Load $Z$.*

For the last test, an imbalance was introduced in the local load $Z$ (keeping the grid unbalanced) to evaluate the performance of the proposed control in this type of scenarios. While phases A and B operate at the value that had been previously used (i.e., 24.2 Ω, see Table 1), and imbalance was introduced in the phase C, which was operated as an open circuit.

Fig. 15 presents $V^-$ for the experimental test. The results show that the imbalance in the local load increases significantly the value of the negative-sequence voltage before the control strategy activation. A value of $V^- = 9.5\ V$ is observed. However, once the control strategy is activated at $t = 0.2$ s, a complete elimination of the negative-sequence voltage is observed.

These experimental tests show that the proposed control strategy eliminates effectively the negative-sequence voltage regardless the origin of the imbalance (it can be produced by the grid, by an unbalanced grid impedance, by an unbalanced local local or by the combination of some of all of these characteristics). Also, that the level of the imbalance does not affect the main dynamic properties of the negative-sequence voltage elimination.

## 7 Conclusion

A control strategy for the negative-sequence voltage elimination for distributed generators operating in grid-feeding mode has been presented in this paper. Compared with previous control strategies, the proposal presents superior operational features such as: (a) offers the possibility to set directly a desired value of reduction of the negative-sequence voltage, (b) the design of its control parameters does not require a prior in-depth knowledge of the grid characteristic to guarantee excellent dynamic and steady-state properties, (c) guarantees a complete elimination of the negative-sequence voltage in different imbalance scenarios.

A pseudo-code has been presented to clarify aspects related to the implementation as well as a flowchart to better understanding the processing stages of the signals. In addition, a closed-loop modeling has been derived based on a complex transfer function approach, from which mathematical expression was derived to calculate the system stability margins and control design guidelines. Experimental results were reported, to verify the accuracy of the modeling and the superior operational features of the proposed strategy.

Future work will be focus on the extension of this control strategy for distributed generators operating in grid-forming mode. Also, control schemes based on distributed communication systems will be explored to guarantee voltage quality objectives in microgrids with multiple DG systems.

## 8 References


1 Adefarati, T., Bansal, R.C.: 'Integration of renewable distributed generators into the distribution system: a review', *IET Ren Power Gen*, 2016, **10**, (7), pp. 873–884

2 Cheng, Z., Duan, J., Chow, M.: 'To centralize or to distribute: That is the question: A comparison of advanced microgrid management systems', *IEEE Ind Electron Mag*, 2018, **12**, (1), pp. 6–24

3 Parhizi, S., Lotfi, H., Khodaei, A., Bahramirad, S.: 'State of the art in research on microgrids: A review', *IEEE Access*, 2015, **3**, pp. 890–925

4 Muhanji, S.O., Muzhikyan, A., Farid, A.M.: 'Distributed control for distributed energy resources: Long-term challenges and lessons learned', *IEEE Access*, 2018, **6**, pp. 32737–32753

5 Zeng, Z., Yang, H., Guerrero, J.M., Zhao, R.: 'Multi-functional distributed generation unit for power quality enhancement', *IET Power Electron*, 2015, **8**, (3), pp. 467–476
6 Ali, Z., Christofides, N., Hadjidemetriou, L., Kyriakides, E.: 'Multi-functional distributed generation control scheme for improving the grid power quality', *IET Power Electron*, 2019, **12**, (1), pp. 30–43
7 Miret, J., Garnica, M.A., Castilla, M., Garcia de Vicuña, J.L., Camacho, A.: 'PI-based controller for low-power distributed inverters to maximise reactive current injection while avoiding over voltage during voltage sags', *IET Power Electron*, 2019, **12**, (1), pp. 83–91
8 Von Jouanne, A., Banerjee, B.: 'Assessment of voltage unbalance', *IEEE Trans Power Del*, 2001, **16**, (4), pp. 782–790
9 Song, Y., Wang, B.: 'Survey on reliability of power electronic systems', *IEEE Trans Power Electron*, 2013, **28**, (1), pp. 591–604
10 Dai, Z., Lin, H., Yin, H., Qiu, Y.: 'A novel method for voltage support control under unbalanced grid faults and grid harmonic voltage disturbances', *IET Power Electron*, 2015, **8**, (8), pp. 1377–1385
11 'IEEE Standard for Interconnecting Distributed Resources with Electric Power Systems: 1547-2003'. (IEEE Standards Board, 2003)
12 Wang, Y.J.: 'Analysis of effects of three-phase voltage unbalance on induction motors with emphasis on the angle of the complex voltage unbalance factor', *IEEE Trans Energy Convers*, 2001, **16**, (3), pp. 270–275
13 Lee, K., Venkataramanan, G., Jahns, T.M.: 'Modeling effects of voltage unbalances in industrial distribution systems with adjustable-speed drives', *IEEE Trans Ind Appl*, 2008, **44**, (5), pp. 1322–1332
14 Aree, P.: 'Effects of unbalanced voltage on induction motor operating points under different load torque profiles', *2016 13th Int Conference on Electrical Engineering/Electronics, Computer, Telecommunications and Information Technology ECTI-CON*, 2016, pp. 1–4
15 Castilla, M., Miret, J., Sosa, J.L., Matas, J., d. VicuÃśa, L.G.: 'Grid-fault control scheme for three-phase photovoltaic inverters with adjustable power quality characteristics', *IEEE Trans on Power Electron*, 2010, **25**, (12), pp. 2930–2940
16 Roscoe, A.J., Finney, S.J., Burt, G.M.: 'Tradeoffs between AC power quality and DC bus ripple for 3-phase 3-wire inverter-connected devices within microgrids', *IEEE Trans Power Electron*, 2011, **26**, (3), pp. 674–688
17 Xiao, L., Huang, S., Lu, K.: 'DC-bus voltage control of grid-connected voltage source converter by using space vector modulated direct power control under unbalanced network conditions', *IET Power Electron*, 2013, **6**, (5), pp. 925–934
18 Graovac, D., Katic, V., Rufer, A.: 'Power quality problems compensation with universal power quality conditioning system', *IEEE Trans Power Del*, 2007, **22**, (2), pp. 968–976
19 Singh, B., Solanki, J.: 'An implementation of an adaptive control algorithm for a three-phase shunt active filter', *IEEE Trans Ind Electron*, 2009, **56**, (8), pp. 2811–2820
20 George, S., Agarwal, V.: 'A DSP based optimal algorithm for shunt active filter under nonsinusoidal supply and unbalanced load conditions', *IEEE Trans Power Electron*, 2007, **22**, (2), pp. 593–601
21 Montero, M.I.M., Cadaval, E.R., Gonzalez, F.B.: 'Comparison of control strategies for shunt active power filters in three-phase four-wire systems', *IEEE Trans Power Electron*, 2007, **22**, (1), pp. 229–236
22 Castilla, M., Miret, J., Camacho, A., Matas, J., de Vicuña, L.G.: 'Voltage support control strategies for static synchronous compensators under unbalanced voltage sags', *IEEE Trans Ind Electron*, 2014, **61**, (2), pp. 808–820
23 Li, Y.W., Vilathgamuwa, D.M., Loh, P.C.: 'A grid-interfacing power quality compensator for three-phase three-wire microgrid applications', *IEEE Trans Power Electron*, 2006, **21**, (4), pp. 1021–1031
24 Alepuz, S., Busquets-Monge, S., Bordonau, J., Martinez-Velasco, J.A., Silva, C.A., Pontt, J., et al.: 'Control strategies based on symmetrical components for grid-connected converters under voltage dips', *IEEE Trans Ind Electron*, 2009, **56**, (6), pp. 2162–2173
25 Lee, C., Hsu, C., Cheng, P.: 'A low-voltage ride-through technique for grid-connected converters of distributed energy resources', *IEEE Trans Ind Appl*, 2011, **47**, (4), pp. 1821–1832
26 Wang, F., Duarte, J.L., Hendrix, M.A.M.: 'Pliant active and reactive power control for grid-interactive converters under unbalanced voltage dips', *IEEE Trans Power Electron*, 2011, **26**, (5), pp. 1511–1521
27 Miret, J., Camacho, A., Castilla, M., de Vicuña, L.G., Matas, J.: 'Control scheme with voltage support capability for distributed generation inverters under voltage sags', *IEEE Tran Power Electron*, 2013, **28**, (11), pp. 5252–5262
28 Camacho, A., Castilla, M., Miret, J., Guzman, R., Borrell, A.: 'Reactive power control for distributed generation power plants to comply with voltage limits during grid faults', *IEEE Trans Power Electron*, 2014, **29**, (11), pp. 6224–6234
29 Nejabatkhah, F., Li, Y.W., Wu, B.: 'Control strategies of three-phase distributed generation inverters for grid unbalanced voltage compensation', *IEEE Trans Power Electron*, 2016, **31**, (7), pp. 5228–5241
30 Jia, J., Yang, G., Nielsen, A.H.: 'A review on grid-connected converter control for short-circuit power provision under grid unbalanced faults', *IEEE Trans Power Del*, 2018, **33**, (2), pp. 649–661
31 Camacho, A., Castilla, M., Miret, J., Vasquez, J.C., Alarcon-Gallo, E.: 'Flexible voltage support control for three-phase distributed generation inverters under grid fault', *IEEE Trans Ind Electron*, 2013, **60**, (4), pp. 1429–1441
32 Camacho, A., Castilla, M., Miret, J., Borrell, A., de Vicuña, L.G.: 'Active and reactive power strategies with peak current limitation for distributed generation inverters during unbalanced grid faults', *IEEE Trans Ind Electron*, 2015, **62**, (3), pp. 1515–1525
33 Sosa, J.L., Castilla, M., Miret, J., Matas, J., Al.Turki, Y.A.: 'Control strategy to maximize the power capability of PV three-phase inverters during voltage sags', *IEEE Trans Power Electron*, 2016, **31**, (4), pp. 3314–3323
34 López, M.A.G., de Vicuña, J.L.G., Miret, J., Castilla, M., Guzmán, R.: 'Control strategy for grid-connected three-phase inverters during voltage sags to meet grid codes and to maximize power delivery capability', *IEEE Trans Power Electron*, 2018, **33**, (11), pp. 9360–9374
35 Duesterhoeft, W.C., Schulz, M.W., Clarke, E.: 'Determination of instantaneous currents and voltages by means of alpha, beta, and zero components', *Transactions of the American Institute of Electrical Engineers*, 1951, **70**, (2), pp. 1248–1255
36 Rodríguez, P., Teodorescu, R., Candela, I., Timbus, A.V., Liserre, M., Blaabjerg, F. 'New positive-sequence voltage detector for grid synchronization of power converters under faulty grid conditions'. In: 37th IEEE Power Electron. Specialists Conference. (, 2006. pp. 1–7
37 Rodríguez, P., Luna, A., Muñoz.Aguilar, R.S., Etxeberria.Otadui, I., Teodorescu, R., Blaabjerg, F.: 'A stationary reference frame grid synchronization system for three-phase grid-connected power converters under adverse grid conditions', *IEEE Trans Power Electron*, 2012, **27**, (1), pp. 99–112
38 Rodriguez, P., Timbus, A.V., Teodorescu, R., Liserre, M., Blaabjerg, F.: 'Flexible active power control of distributed power generation systems during grid faults', *IEEE Trans Ind Electron*, 2007, **54**, (5), pp. 2583–2592
39 Matas, J., Castilla, M., Miret, J., de Vicuña, L.G., Guzman, R.: 'An adaptive prefiltering method to improve the speed/accuracy tradeoff of voltage sequence detection methods under adverse grid conditions', *IEEE Trans Ind Electron*, 2014, **61**, (5), pp. 2139–2151
40 Yazdani, A., Iravani, R.: 'Voltage-sourced converters in power systems: modeling, control, and applications'. (John Wiley & Sons, 2010)
41 Rodriguez, P., Luna, A., Candela, I., Mujal, R., Teodorescu, R., Blaabjerg, F.: 'Multiresonant frequency-locked loop for grid synchronization of power converters under distorted grid conditions', *IEEE Trans Ind Electron*, 2011, **58**, (1), pp. 127–138
42 Castilla, M., Miret, J., Camacho, A., de Vicuña, L.G., Matas, J.: 'Modeling and design of voltage support control schemes for three-phase inverters operating under unbalanced grid conditions', *IEEE Trans Power Electron*, 2014, **29**, (11), pp. 6139–6150
43 Harnefors, L.: 'Modeling of three-phase dynamic systems using complex transfer functions and transfer matrices', *IEEE Trans Ind Electron*, 2007, **54**, (4), pp. 2239–2248
44 Stankovic, A.M., Sanders, S.R., Aydin, T.: 'Dynamic phasors in modeling and analysis of unbalanced polyphase AC machines', *IEEE Trans Energy Convers*, 2002, **17**, (1), pp. 107–113
45 Guo, X., Lu, Z., Wang, B., Sun, X., Wang, L., Guerrero, J.M.: 'Dynamic phasors-based modeling and stability analysis of droop-controlled inverters for microgrid applications', *IEEE Trans Smart Grid*, 2014, **5**, (6), pp. 2980–2987
46 Agashe, S.: 'A new general Routh-like algorithm to determine the number of RHP roots of a real or complex polynomial', *IEEE Trans Autom Control*, 1985, **30**, (4), pp. 406–409
47 Bodson, M. 'The complex Hurwitz test for the stability analysis of induction generators'. In: Proceedings of the 2010 American Control Conference. (, 2010. pp. 2539–2544
48 Asiminoaei, L., Teodorescu, R., Blaabjerg, F., Borup, U.: 'Implementation and test of an online embedded grid impedance estimation technique for PV inverters', *IEEE Transactions on Industrial Electronics*, 2005, **52**, (4), pp. 1136–1144
49 Liserre, M., Blaabjerg, F., Teodorescu, R.: , *IEEE*, ,
50 Cobreces, S., Bueno, E.J., Pizarro, D., Rodriguez, F.J., Huerta, F.: 'Grid impedance monitoring system for distributed power generation electronic interfaces', *IEEE Transactions on Instrumentation and Measurement*, 2009, **58**, (9), pp. 3112–3121
51 Hoffmann, N., Fuchs, F.W.: 'Minimal invasive equivalent grid impedance estimation in inductiveâĂŞresistive power networks using extended kalman filter', *IEEE Transactions on Power Electronics*, 2014, **29**, (2), pp. 631–641
52 Ghanem, A., Rashed, M., Sumner, M., Elsayes, M.A., Mansy, I.I.I.: 'Grid impedance estimation for islanding detection and adaptive control of converters', *IET Power Electronics*, 2017, **10**, (11), pp. 1279–1288


# 9 Appendix

## 9.1 Closed-Loop Complex Transfer Function

The complete expression of the closed-loop complex transfer function is obtained inserting (17), (19) and (21) in (22). Thus, $F(s)$ can be expressed as

$$F = \frac{(a_0 + jb_0)s^3 + (a_1 + jb_1)s^2 + (a_2 + jb_2)s + (a_3 + jb_3)}{c_0 s^3 + (c_1 + jd_1)s^2 + (c_2 + jd_2)s + (c_3 + jd_3)} \tag{24}$$

being

$$\begin{aligned} a_0 &= K_r L_L \\ b_0 &= K_i L_L \\ a_1 &= K_r(R_L + 2L_L\xi\omega) + K_i L_L \omega \end{aligned}$$

$$
\begin{aligned}
b_1 &= -K_r L_L \omega + K_i (R_L + 2L_L \xi \omega) \\
a_2 &= K_r (2R_L \xi \omega + L_L \omega^2) + 2K_i L_L \xi \omega^2 \\
b_2 &= -2K_r L_L \xi \omega^2 + K_i (2R_L \xi \omega + L_L \omega^2) \\
a_3 &= K_r R_L \omega^2 + K_i L_L \omega^3 \\
b_3 &= -K_r L_L \omega^3 + K_i R_L \omega^2 \\
c_0 &= 1 \\
c_1 &= 2\xi\omega + K_r L_L \xi \omega \\
d_1 &= \omega + K_i L_L \xi \omega \\
c_2 &= \omega^2 + K_r R_L \xi \omega + 2K_i L_L \xi \omega^2 \\
d_2 &= 2\xi\omega^2 - 2K_r L_L \xi \omega^2 + K_i R_L \xi \omega \\
c_3 &= -K_r L_L \xi \omega^3 + K_i R_L \xi \omega^2 \\
d_3 &= \omega^3 - K_r R_L \xi \omega^2 - K_i L_L \xi \omega^3.
\end{aligned}
$$